The *Chlamydia* type III effector TarP alters the dynamics and organization of host focal adhesions

António T. Pedrosa[a,b], Ana T. Nogueira[a,b], Tristan R. Thwaites[b], Jesse Aaron[c], Teng-Leong Chew[c], and Rey A. Carabeo[a,1]

[a]School of Molecular Biosciences, College of Veterinary Medicine, Washington State University, Pullman, WA 99164; [b]Bacteriology Section, Programme in Microbiology, Institute of Medical Sciences, University of Aberdeen, Aberdeen, UK AB25 2ZD; [c]Advanced Imaging Center, Janelia Research Campus, Howard Hughes Medical Institute, Ashburn, VA 20147

Corresponding author:
Rey A. Carabeo
School of Molecular Biosciences
College of Veterinary Medicine
Washington State University
Pullman, WA 99164
(509) 335-7788
Mail to: rcarabeo@vetmed.wsu.edu

Keywords: *Chlamydia*, Focal adhesion, Pathogenesis, FA modulation, Adhesion, iPALM

Abstract

Bacterial infection of mucosal epithelial cells triggers cell exfoliation to limit the dissemination of infection within the tissue. Therefore, mucosal pathogens must possess strategies to counteract cell extrusion in response to infection. Chlamydia trachomatis spends most of its intracellular development in the non-infectious form. Thus, premature host cell extrusion is detrimental to the pathogen. We demonstrate that C. trachomatis alters the dynamics of focal adhesions. Live-cell microscopy showed that focal adhesions in C. trachomatis-infected cells displayed increased stability. In contrast, focal adhesions in mock-infected cells readily disassembled upon inhibition of myosin II by blebbisttin. Super-resolution microscopy revealed a reorganization of paxillin and FAK in infected cells. Ectopically expressed type III effector TarP localized to focal adhesions, leading to their stabilization and reorganization in a vinculin-dependent manner. Overall, the results indicate that C. trachomatis possesses a dedicated mechanism to regulate host cell focal adhesion dynamics.

Introduction

Bacterial infection of mucosal epithelial cells triggers the antimicrobial defence strategy of cell exfoliation and apoptosis induction (reviewed in: Kim *et al.*, 2010). The controlled extrusion of damaged host cells and colonizing pathogens requires the degradation of cell adhesion factors.

In epithelial cells, focal adhesions and hemidesmosomes are primarily responsible for attachment to the extracellular matrix, and their assembly and turnover are exquisitely regulated at multiple levels, by kinases, phosphatases, protein-protein interactions, internalization of components, and degradation (Borradori and Sonnenberg, 1999; Geiger *et al.*, 2001; Zaidel-Bar *et al.*, 2007). Disruption of one or more of these regulatory processes alters the adhesion dynamics and properties of the cells.

One strategy employed by bacteria to neutralize exfoliation relies on the precise targeting of one or more component of the focal adhesion proteome. The best-characterized example is that of *Shigella*, which neutralizes epithelial extrusion to colonize the epithelium efficiently. It does so by delivering the OspE effector by the type III secretion system (T3SS). This protein reinforces host cell adherence to the basement membrane by interacting with integrin-linked kinase (ILK), a serine/threonine kinase that is part of the focal adhesome (Zaidel-Bar *et al.*, 2007). A consequence of the OspE-ILK interaction is an increased surface expression of β1-integrin, which in turn promotes focal adhesion (FA) assembly. In addition, the OspE-ILK complex stabilizes the focal adhesions (FAs) by reducing phosphorylation of focal adhesion kinase (FAK) at a functionally important Tyr397 residue and of paxillin. Inhibition of both phosphorylation events has been shown to induce FA disassembly (Kim *et al.*, 2009). Interestingly, some EPEC and EHEC strains, as well as *Citrobacter rodentium* possess the effector EspO, which shares strong homology with OspE (reviewed in Vossenkämper, Macdonald and Marchès, 2011; Morita-Ishihara *et al.*, 2013). As such, it is conceivable that these pathogens also reinforce adherence of the infected epithelial cells to secure an infectious foothold. The EspZ effector of EPEC and EHEC has been shown to reduce cell death and detachment *in vitro* (Shames *et al.*, 2010). EspZ binds the transmembrane glycoprotein CD98 and enhances its effect on β1-integrin signalling and cell survival via activation of FAK(Shames *et al.*, 2010).It is possible that EspO and EspZ may cooperate to confer enhanced

adhesion of the host epithelial cells to the extracellular matrix. Finally, through interaction with human carcino-embryonic antigen-related cell adhesion molecules (CEACAM), bacterial pathogens such as *Neisseria gonorrhoeae*, *Neisseria meningitidis*, *Moraxella catarrhalis*, and *Haemophilus influenzae* can activate β1-integrin signalling and inhibit epithelial cell detachment (reviewed in: Kim *et al.*, 2010). Despite numerous examples of pathogens manipulating host cell adhesion, the details of the mechanisms remain uncharacterized.

Chlamydiae are obligate intracellular pathogens that are distinguished by their biphasic developmental cycle that alters between the infectious elementary body (EB), and the replicative, but non-infectious reticulate body (RB). At late time points, the non-infectious RBs convert back to EBs to produce infectious particles for the next round of infection. The entire intracellular growth cycle of *Chlamydia* takes ~48–96 h and occurs within a membrane-bound inclusion, and most of it is spent in the non-infectious RB form. Thus, it is essential that the adhesion of the infected cells to the epithelium is sustained during chlamydial development to enable the differentiation of the non-infectious RBs to the infectious and stable elementary bodies (EBs) (reviewed in AbdelRahman and Belland, 2005). This means that *Chlamydia* must evade a host of antimicrobial defences, including epithelial extrusion.

Previous works by Kumar and Valdivia (2008) and Heymann *et al.*, (2013) described the loss of motility of *Chlamydia*-infected epithelial cells. Heymann *et al.*, (2013) attributed this to the chlamydial inhibition of Golgi polarization that occurs at >24 h post-infection, leading to loss of directional migration. In this report, we offer an alternate and possibly complementary mechanism of FA stabilization, which could lead to an increase of host-cell adhesion to the extracellular matrix (ECM), thus culminating in loss of motility as previously described (Kumar and Valdivia, 2008; Heymann *et al.*, 2013). Using quantitative confocal and live-cell imaging and super-resolution microscopy, we describe the various aspects of chlamydial modulation of FAs, such as increased number, enhanced stability, and reorganization, which is initiated at early time points and maintained throughout infection. Importantly, we demonstrate a previously unreported post-invasion role for the T3SS effector TarP in influencing these properties. Focal adhesions in *Chlamydia*-infected or TarP-expressing cells displayed unusual resistance to disassembly induced by treatment

with blebbistatin, a specific inhibitor of myosin II. In addition, the vertical organizations of the FA-associated proteins, paxillin and FAK were significantly altered in both infected and TarP-expressing cells, indicating a crucial role for the T3SS effector. Furthermore, the FA-stablizing role of TarP was dependent on vinculin, which was confirmed by the inability of TarP with deleted vinculin-binding sites to inhibit FA turnover. Overall, the results indicate that *Chlamydia* has a dedicated mechanism of inhibiting epithelial cell extrusion during its intracellular development.

Results

Infected cells exhibited increased resistance to detachment

To be able to establish infection in mucosal epithelium *C. trachomatis* needs to overcome the extrusion defence mechanism of the epithelial cells. A mild trypsin treatment was used to determine if *C. trachomatis* serovar L2 (CtrL2) affected host cell adhesion. Mock- and CtrL2-infected cells were treated with 0.01% trypsin and fixed with 4% PFA at predetermined time points up to 35 min post-trypsin treatment (Figure 1). A qualitative difference between the infected sample (bottom panel Figure 1A), and mock-infected sample (top panel Figure 1A) was apparent within 10 min of trypsin treatment. The infected cell monolayer of the CtrL2-infected cells was unaltered up to 30 min after trypsin treatment. In contrast, the mock-infected monolayer developed gaps starting at 10 min of trypsinisation with almost complete loss of cells at 35 min. The number of nuclei in images corresponding to two independent experiments was quantified using the FIJI software (Figure 1B). Data are represented as box-and-whisker plots. The number of nuclei was normalized to the average number of nuclei at 0 min of treatment for each sample. A significant decrease in number of nuclei in the mock-infected sample was observed starting at 10 min post-trypsinization. Alternatively, only a marginal difference was observed in the CtrL2-infected sample at the 35min time point. Furthermore, a significant difference between the mock- and CtrL2-infected samples was observed at 10 min post-trypsin treatment, and was maintained for the length of the experiment. Resistance to trypsinization was also observed in cells seeded at low confluence (Movie S1). These results suggested that *Chlamydia* conferred resistance to detachment by trypsinization, possibly by enhancing the adhesion of the host cell to the substrate.

Infected cells exhibited focal adhesion changes

The enhanced adhesion of infected cells observed could be due to changes in the number and size of focal adhesions. Focal adhesions are important integrin-based structures that anchor the cell to the ECM. Three different FAs markers were used to monitor the number and turnover dynamics. Cells were either mock- or CtrL2-infected and then fixed at 8 and 20 h post-infection (hpi). Samples were then stained for paxillin, vinculin, or FAK phoshphorylated at Tyr397 (pFAK-Y^{397}) (Figure 2A,

2B and S1A). FIJI image software was used to quantify the number of FAs in images obtained by confocal microscopy, and data represented as box-and-whisker plots (Figure 2C, 2D and S1B). In mock-infected cells stained for vinculin, an average number of 34 ± 16 (n=46) FAs were observed. This was significantly lower than vinculin-marked FAs in CtrL2-infected cells at both 8 and 20 hpi [79 ± 63 (n=45, p-value ≤ 0.001; Wilcoxon rank sum test) and 75 ± 36 (n=45, p-value ≤ 0.001; Wilcoxon rank sum test), respectively]. Similarly, a significant increase in FA numbers was observed at 20 hpi between mock- and CtrL2-infected cells for FAs marked with paxillin [32 ± 11 (n=34) vs.59 ± 28 (n=18, p-value ≤ 0.001; Wilcoxon rank sum test), respectively]. The same significant increase in CtrL2-infected cells was observed for pFAK-Y^{397}-marked FAs [56 ± 22 (n=40) vs 75 ± 36 (n=45, p-value ≤ 0.001; Wilcoxon rank sum test), respectively]. A similar trend was observed at an earlier time point of infection (8 hpi) for paxillin between mock- and CtrL2-infected cells [32 ± 11 (n=34) vs. 59 ± 27 (n=24, p-value ≤ 0.001; Wilcoxon rank sum test), respectively] and pFAK-Y^{397} [56 ± 22 (n=40) vs. 88 ± 49 (n=26, p-value ≤ 0.001; Wilcoxon rank sum test), respectively]. No significant difference was observed between the CtrL2 8 hpi and the CtrL2 20 hpi time points, for the markers mentioned above. Further studies using the focal adhesion marker vinculin revealed that FA numbers significantly increased as early as 2 hpi [(34 ± 16 (n=46) vs. 68 ± 46 (n=43, p-value ≤ 0.001; Wilcoxon rank sum test)] (Figure S1C and S1D).

The relatively early time point (2 hpi) of FA modulation by CtrL2 indicated that a pre-synthesized protein, possibly a T3SS effector associated with elementary bodies might be involved. To test this hypothesis CtrL2 infection was performed in the presence of chloramphenicol to inhibit *de novo* protein synthesis, yet allowing translocation of pre-synthesized proteins in the EB. For this experiment vinculin and paxillin were used as FA markers (Figure 2A and 2B, respectively). Images obtained by confocal microscopy were quantified using FIJI image software, and data was represented using box-and-whisker plots (Figure 2C and 2D). The results obtained were comparable with the non-chloramphenicol-treated samples. At 8 hpi, significant increase in FA numbers between mock- and CtrL2-infected cells was observed for vinculin- [34 ± 16 (n=46) vs. 62 ± 28, (n=35, p-value ≤ 0.001; Wilcoxon rank sum test), respectively] and paxillin-stained samples [32 ± 11 (n=34) vs. 76 ± 40, (n=41, p-value ≤ 0.001; Wilcoxon rank sum test) , respectively]. A

similar significant increase in vinculin- [34 ± 16 (n=46) vs. 76 ± 40, (n=41, p-value ≤ 0.001; Wilcoxon rank sum test), respectively] and paxillin-stained (32 ± 11 (n=34) vs. 49 ± 24 (n=40, p-value ≤ 0.001; Wilcoxon rank sum test) , respectively] FA numbers was observed at 20 hpi. Remarkably, chloramphenicol treatment did not affect the FA numbers of CtrL2-infected cells, indicating that the protein(s) responsible for changes to focal adhesions at 8 and 20 hpi was already present in EBs. Additionally, inoculation with heat-killed CtrL2 EBs did not increase FA numbers (Figure S1C and S1D) at 8 and 20 hpi.

Focal adhesion modulation was neither *Chlamydia* species nor host cell type-dependent. A qualitative increase in FAs was also observed in HaCaT and MEFs cell lines infected with CtrL2 for 20 h (Figure S2A-S2D). An increase in FAs marked with pFAK-Y^{397} was also observed in Cos7 cells infected with *Chlamydia caviae* at 8 hpi (Figure S1E and S1F). These results suggested that FA modulation might be conserved in the genus Chlamydia, which would be consistent with this feature being an important adaptive mechanism to infection of the high-turnover mucosal epithelia.

Focal adhesion changes in infected cells are associated with increased stability

Focal adhesion numbers are influenced by the dynamics of biogenesis and turnover (Nagano *et al.*, 2012; Kim and Wirtz, 2013). We investigated the rates of recruitment and turnover of three FA markers (transiently transfected paxillin-EGFP, FAK-EGFP or vinculin-Venus) in CtrL2- or mock-infected NIH3T3 cells seeded on fibronectin using quantitative live-cell TIRF microscopy (Movies S2-S4). Individual FAs from time-lapse imaging were analyzed using the Focal Adhesion Analysis Server (FAAS) (Berginski and Gomez, 2013) (Figures 3A, 3B, 3C). With images from each frame indicated by a different colour, the difference in the turnover and spatial dynamics of FAs marked by paxillin-EGFP between CtrL2 and mock-infected cells was observed (Figure 3A). The same was observed for FAK-EGFP- and vinculin-Venus-labelled FAs (Figure S2E). Figures 3B and 3C illustrate the differences in the recruitment and turnover rates for over 3000 FAs analyzed per condition (data represented using box-and-whisker plots). We observed slower turnover rates for FAs of CtrL2-infected cells when compared to the mock-infected samples. The average turnover rate for FAK-EGFP in mock-infected cells was 0.047 ± 0.050 intensity/min (n=799) *vs*. CtrL2-

185 infected cells 0.031 ± 0.035 intensity/min (n=761) (p-value ≤ 0.001, Wilcoxon rank sum test). For
186 paxillin-EGFP, the turnover rates for mock-infected and CtrL2-infected cells were 0.045 ± 0.046
187 intensity/min (n=593) vs. 0.035 ± 0.041 intensity/min (n=750) (p-value ≤ 0.001, Wilcoxon rank sum
188 test), respectively. Finally, the turnover rate of vinculin-Venus for mock-infected cells was 0.030 ±
189 0.030 intensity/min (n=955), while that for CtrL2-infected cells was 0.024 ± 0.023 intensity/min
190 (n=1113) (p-value ≤ 0.001, Wilcoxon rank sum test). Interestingly, the rates of recruitment for the
191 same FA markers in CtrL2-infected cells were slower than those of mock-infected controls. For
192 FAK-EGFP, mock- vs. CtrL2-infected samples had turnover rates of 0.048 ± 0.040 intensity/min
193 (n=656) and 0.038 ± 0.030 intensity/min (n=584) (p-value ≤ 0.001, Wilcoxon rank sum test),
194 respectively. Paxillin-EGFP yielded rates of 0.055 ± 0.048 intensity/min (n=644) and 0.035 ± 0.035
195 intensity/min (n=773) (p-value ≤ 0.001, Wilcoxon rank sum test), for mock- and CtrL2-infected
196 samples, respectively. Finally, vinculin-Venus rates were 0.049 ± 0.037 intensity/min (n=654; mock-
197 infected) and 0.031 ± 0.030 intensity/min (n=842; CtrL2-infected) p-value ≤ 0.001, Wilcoxon rank
198 sum test) (Figure 3C). Because of the nature of FAs assembly, disassembly and protein recycling,
199 the reduced turnover might account for the reduced recruitment rates observed.
200
201 *Focal adhesions of infected cells exhibit resistance to disassembly induced by inhibitors of myosin II*
202 We further explored the stability phenotype exhibited by the FAs in CtrL2-infected cells. Specifically,
203 we tested if they remained susceptible to the destabilizing effects of blebbistatin, a specific myosin II
204 inhibitor (Straight *et al.*, 2003). Myosin II function is to increase the mechanostress on FAs via its
205 action on the stress fibers, thus promoting their stability (Liu *et al.*, 2010). At 7 hpi, cells were
206 treated with 10 µM blebbistatin for 1 h. Fixed cells were stained with an antibody against paxillin. As
207 expected, after treatment with blebbistatin, control cells lost paxillin-containing FAs and F-actin-rich
208 stress fibers (SFs), as expected, whereas CtrL2-infected cells treated with blebbistatin lost the SFs,
209 but retained the FAs (Figures 3D).
210 We showed above that increased FA numbers did not require *de novo* chlamydial protein
211 synthesis. Here, blebbistatin resistance of focal adhesions of CtrL2-infected cells was monitored in
212 the presence or absence of chloramphenicol at 8 hpi (Figure 3E and S6), and remarkably, the FAs

of infected cells remained resistant to blebbistatin (Figure 3E). These results suggested that possibly the same EB factor that modulated FAs numbers could also be modulating FA resistance to blebbistatin. In addition, FAs displayed the same blebbistatin-resistant phenotype at 20 hpi regardless of chloramphenicol treatment (Figure S3A and S3B).

TarP mimics Chlamydia's modulation of focal adhesions numbers

To gain mechanistic insight into FA modulation by *Chlamydia* infection, we investigated the role of the T3SS effector TarP, which was an excellent candidate for the chloramphenicol-insensitive focal adhesion stabilizing factor. TarP interacts with FAK via the leucine-aspartic acid (LD) motif (residues LExLLPxLRAHL) and with vinculin via the two vinculin-binding sites (residues LxxAAxNVTxxLS), which comprise TarP's vinculin binding domain (VBD) in the C. trachomatis serovar L2 orthologue (Thwaites *et al.*, 2014, 2015). Additionally, when transiently transfected in eukaryotic cells TarP localizes at the FAs (Figure S3C). Together, these properties of TarP make a strong case for a role in FA modulation. We sought to determine the extent of TarP contribution to the FAs phenotype observed in CtrL2-infected cells, e.g. increased numbers, assembly and disassembly rates and resistance to blebbistatin. Various constructs of CtrL2 TarP ortholog fused with mturquoise2 fluorescence protein (Figure 4A) were transiently transfected in Cos7 cells for 20 h. The cells were fixed and stained with phalloidin and paxillin to visualize SFs and FAs, respectively. In this experiment, we monitored simultaneously in transfected cells the localization of TarP constructs at FAs, and the potential changes in FA numbers.

First, we evaluated the ability of the different TarP constructs to specifically localize to the site of FAs (Figure 4B). We observed that ectopically expressed $TarP^{1\text{-}1006\Delta625\text{-}650}$ (in green) localized to the paxillin-marked FAs (in red). It is important to note that $TarP^{1\text{-}1006\ \Delta625\text{-}650}$, which lacks the proline-rich domain, was indistinguishable from intact TarP with regards to the recruitment of FAK and vinculin at the plasma membrane (Thwaites *et al.*, 2014, 2015) or its localization to the FAs (Figure S3C). $TarP^{1\text{-}1006\Delta625\text{-}650}$ was less prone to aggregate in the cytosol when ectopically expressed. $TarP^{829\text{-}929}$, which is comprised of the FAK binding domain (LD) localized to both FAs and SFs, while $TarP^{1\text{-}1006\Delta625\text{-}650}$, $TarP^{829\text{-}1006}$, and $TarP^{905\text{-}1006}$ localized to FAs only. The common

domain retained by these FA-localizing TarP derivatives was the vinculin-binding domain (VBD), indicating that this domain is essential for specific localization to the host cell FAs. The TarP$^{1\text{-}829\Delta625\text{-}650}$ derivative, which contained only the annotated actin-binding domain did not localize to FAs possibly, reinforcing the role of the VBD in the FA localization of TarP.

Using confocal microscopy images, we were able to quantify the total FA number in cells ectopically expressing the various TarP constructs described above. In this series of experiments, we wanted to determine if TarP alone could modulate FA numbers. FAs were enumerated using FIJI as previously described (see Materials and Methods for details), and data presented as a box-and-whiskers plot (Figure 4C). The N1-mturquoise2 empty vector [43 ± 19 (n=26)] was the control and provided the basal value. The quantification revealed that the FA numbers in cells transfected with TarP derivatives harboring the LD or the VBD motifs were statistically significantly increased, with mean values of 106 ± 45 (n=32), p-value ≤ 0.001 (TarP$^{1\text{-}1006\Delta625\text{-}650}$); 70 ± 28 (n=43), p-value ≤ 0.001 (TarP$^{829\text{-}1006}$), 58 ± 16 (n=20), p-value ≤ 0.001 (TarP$^{829\text{-}929}$), and 68 ± 22 (n=19), p-value ≤ 0.001 (TarP$^{905\text{-}1006}$). Additionally, the non-FA-localizing TarP$^{1\text{-}829\Delta625\text{-}650}$ construct did not differ from the control empty vector [47 ± 20 (n=29) vs. 43 ± 19 (n=26), p-value > 0.05)]. Wilcoxon rank sum test was used to determine statistical significance.

Interestingly, we observed that TarP$^{1\text{-}1006\Delta625\text{-}650}$ produced more FAs than other TarP-derived constructs, which suggested that other domains at the N-terminal portion of the protein is necessary for a greater modulation of FAs. In addition, the VBD motif is important for both increased numbers of and localization to focal adhesions.

TarP modulates focal adhesion stability

We then evaluated the resistance of FAs harboring the different deletion derivatives of TarP to disassembly by a 1 h treatment with 10 μM blebbistatin. We found that TarP$^{1\text{-}1006\Delta625\text{-}650}$, TarP$^{829\text{-}1006}$, and TarP$^{905\text{-}1006}$ derivatives were able to confer resistance to blebbistatin-induced disassembly, as shown by the retention of FAs (Figure 5A). All of these constructs retained the VBD region of TarP. Interestingly, while the TarP$^{829\text{-}929}$ protein, which is composed of the LD domain was able to localize and increase FA numbers, it was ineffective in inducing blebbistatin-resistance, indicating that FA

localization is not sufficient. In other words, FA localization and blebbistatin resistance could be uncoupled. Additionally, these results suggested that the interaction between TarP and vinculin is required to confer FAs resistance to myosin II inhibition.

We also examined the effects of the TarP constructs in the recruitment and turnover rates of paxillin-mCherry-marked FAs (Figure 5B and 5C, respectively) using TIRF microscopy (Movies S5-S10). As described above for CtrL2-infected cells, paxillin recruitment and turnover were both decreased relative to mock-infected control (Figure 3B and 3C). In this experiment, we observed that only TarP$^{1\text{-}1006\Delta625\text{-}650}$ mimicked the kinetics in infected cells. NIH3T3 cells transfected with TarP$^{1\text{-}1006\Delta625\text{-}650}$ yielded the following recruitment and turnover rates: 0.054 ± 0.047 intensity/min (n=577, p-value ≤ 0.001) and 0.045 ± 0.040 intensity/min (n=307, p-value ≤ 0.001), respectively. TarP$^{1\text{-}829\Delta625\text{-}650}$ (retaining the LD, but not the VBD motif) was unable to increase FA numbers (Figure 4C) and confer resistance to blebbistatin treatment (Figure 5A). Also, this TarP construct did not significantly alter the recruitment [0.066 ± 0.050 intensity/min (n=548, p-value ≤ 0.001; Wilcoxon rank sum test)] and turnover rates [0.059 ± 0.048 intensity/min (n=678, p-value > 0.05; Wilcoxon rank sum test)] of paxillin in FAs, when compared to the N1-mturquoise2 empty vector control [recruitment: 0.063 ± 0.044 intensity/min (n=777) and turnover: 0.057 ± 0.038 intensity/min (n=814)]. Surprisingly, no significant difference in recruitment and turnover rates between N1-mturquoise2 and TarP$^{829\text{-}929}$-transfected (LD only) cells [0.066 ± 0.050 intensity/min (n=964, p-value > 0.05; Wilcoxon rank sum test)] and [0.059 ± 0.043 intensity/min (n=1208, p-value > 0.05; Wilcoxon rank sum test)], respectively. Interestingly, TarP$^{929\text{-}1006}$ (VBD only) transfection had the opposite effect of TarP$^{1\text{-}1006\Delta625\text{-}650}$ in the recruitment and turnover rates of paxillin in FAs. An increase in FA recruitment and turnover rates was observed in cells transfected with TarP$^{929\text{-}1006}$ [0.077 ± 0.058 intensity/min (n=618, p-value ≤ 0.01) and 0.067 ± 0.049 intensity/min (n=671, p-value ≤ 0.001), respectively], in comparison with the N1-mturquoise2 control vector. Lastly, for cells transfected with TarP$^{829\text{-}1006}$ an increase of recruitment rate was observed [0.073 ± 0.048 intensity/min (n=1148, p-value ≤ 0.001; Wilcoxon rank sum test)]. However, no significant alteration to the turnover rate between TarP$^{829\text{-}1006}$ [0.059 ± 0.042 intensity/min (n=1616, p-value > 0.05; Wilcoxon rank sum test)] and N1-turquoise2 control vector was observed.

297

298 *Vinculin is required for Chlamydia-induced blebbistatin resistance*

299 In previous experiments, the VBD of TarP was proven to be essential to confer resistance to
300 disassembly via myosin II inhibition using its inhibitor, blebbistatin. To confirm this observation, this
301 resistance phenotype was evaluated in wild type ($vcl^{+/+}$) or vinculin double knock-out ($vcl^{-/-}$) mouse
302 embryo fibroblasts (Figure 6A). As expected when treated with 10 µM of blebbistatin for 1 h mock-
303 infected MEFs $vcl^{+/+}$ and MEFs $vcl^{-/-}$ lost both paxillin-marked FAs and F-actin SFs. However, in
304 CtrL2-infected cells although SFs were lost in both MEFs $vcl^{+/+}$ and $vcl^{-/-}$ MEFs, the FAs in $vcl^{+/+}$
305 were resistant to blebbistatin treatment. The same was not observed in $vcl^{-/-}$ MEFs, which lost FAs
306 despite CtrL2 infection. This indicated that the eukaryotic protein vinculin is required by *Chlamydia*
307 to confer resistance to disassembly by myosin II inhibition.

308 To further implicate TarP-vinculin interaction in FA modulation, $vcl^{+/+}$ and $vcl^{-/-}$ MEFs were
309 transfected with the previously mentioned TarP constructs (Figure 4A). N1-mturquoise2 was used
310 as the control vector for possible side effects of transfection. It should be noted that the various
311 TarP constructs used here behaved similarly in Cos7 and wild type MEFs, with regards to
312 localization to focal adhesion and their ability to confer resistance to blebbistatin-mediated
313 disassembly (Figure S4 vs. Figures 4 and 5). As expected neither a specific localization nor FA
314 resistance to myosin II inhibition was observed in both $vcl^{+/+}$ or $vcl^{-/-}$ MEFs (Figure 6). In contrast,
315 $TarP^{905\text{-}1006}$ (VBD only) showed specific FA localization in $vcl^{+/+}$ MEFs, but this localization was lost
316 in $vcl^{-/-}$ cells. Additionally, resistance to blebbistatin of FAs was only observed in $vcl^{+/+}$ MEFs
317 transfected with $TarP^{905\text{-}1006}$, while FAs in $vcl^{-/-}$ cells transfected with the same construct remained
318 susceptible to blebbistatin treatment (Figure 6). Similarly, $TarP^{1\text{-}1006\Delta625\text{-}650}$ and $TarP^{829\text{-}1006}$ which
319 also specific localized to FAs and were able to confer FA resistance to myosin II inhibition displayed
320 a similar requirement for vinculin (Figure S4).

321

Ectopic expression of TarP partially mimics the reorganization of paxillin and FAK in the focal adhesions of Chlamydia-infected cells

As shown above, TarP localized to focal adhesions in a manner that required the VBD motif. Because FAs are highly organized structures, the insertion of a protein that binds to one or more FA-associated proteins would likely cause changes to the spatial organization. To examine if the localization of TarP within FAs resulted in changes to their organization, we performed super-resolution imaging using interferometric photoactivation and localization microscopy (iPALM) of CtrL2-infected and mock-infected cells expressing paxillin-tdEos, vinculin-tdEos, or FAK-tdEos (Figure 7). Presence of an inclusion in infected cells was confirmed by DIC (Figure S5). The fluorescent protein tdEos is a photoactivated protein allowing the activation of individual fluorescent molecules. This allows to precisely map the coordinates with three-dimensional nanoscale resolution of the photoactivated fluorescent-tagged molecules (Betzig *et al.*, 2006). For cells electroporated with tdEos-tagged constructs 50000 images were acquired per cell for analyses iPALM imaging revealed the vertical distance of paxillin, FAK and vinculin in mock-infected cells to be 50.5 nm (Figure 7A), 40.4 nm (Figure 7C), and 71 nm (Figure 7E), respectively, relative to the gold fiducial marker embedded within the coverslip. These values are consistent with what has been reported for these three FA proteins (Kanchanawong *et al.*, 2010). Unexpectedly, in CtrL2-infected cells, both paxillin-tdEos and FAK-tdEos were redistributed vertically in the FAs, with a peak height of 176.9 nm (Figure 7B) and 96 nm (Figure 7D). Interestingly, vinculin showed no alteration of vertical organization in the CtrL2-infected cells with a peak at 71 nm (Figure 7F), indicating that the reorganization specifically targeted a subset of the FA-associated proteins. The markedly different paxillin and FAK distribution has never been reported for any experimental system.

Next, we investigated the contribution of TarP to this reorganization phenotype. Paxillin-tdEos expression plasmid was co-electroporeted with individual deletion constructs of TarP-FLAG, and iPALM images were obtained and processed to determine changes to the vertical organization. For cells electroporated with Flag-tagged constructs 25000 images were acquired per cell for analyses. We focused on the following TarP constructs: $TarP^{1\text{-}1006\Delta625\text{-}650}$, $TarP^{829\text{-}1006}$ and $TarP^{1\text{-}}$

$^{829\Delta625\text{-}650}$. The first two constructs were able to localize to FAs and increase the numbers of FAs and their level of resistance to blebbistatin. The normalized molecule count distribution data from CtrL2-infected and mock-infected samples were used as reference. As shown in Figure 8A, the peak of pFH-TarP$^{1\text{-}1006\Delta625\text{-}650}$ (228.2 nm) was approximate with that of paxillin-tdEos (240.2) within the same FA (Figure 8B). This mimicked the phenotype observed in CtrL2-infected cells. We also evaluated pFH-TarP$^{829\text{-}1006}$ (Figure 8C), which yielded intermediate phenotypes with regards to FA number (Figure 4B). The protein distribution showed two peaks; one coincided well with the peak for pFH-TarP$^{1\text{-}1006\Delta625\text{-}650}$, and a second in an intermediate position. Monitoring the paxillin-tdEos distribution in the same cells (Figure 8D), we observed segregation to the intermediate pFH-TaRP$^{829\text{-}1006}$ peak and mock-infected peak. A TarP construct lacking LD and the VBD (TarP$^{1\text{-}829\Delta625\text{-}650}$), and thus unable to localize to FAs failed to redistribute paxillin-tdEos (Figure 8E). These data show that LD and VBD domains of TarP could induce an intermediate reorganization phenotype with regards to paxillin. In addition, the intermediate phenotype acquired from the pFH-TaRP$^{829\text{-}1006}$ samples was consistent with its intermediate effects on FA numbers and the hypotheses of other N-terminus domains of TarP being involved in FA modulation. However, as previously noted, these domains, which were presumably retained in the TarP$^{1\text{-}829\Delta625\text{-}650}$, construct would not be able to perform their function in the absence of the FA targeting domains.

Discusion

With a large portion of its intracellular developmental cycle spent in the non-infectious RB form, it is imperative for *Chlamydia trachomatis* and other chlamydial species to develop a strategy to counteract the constant epithelial cell shedding observed *in vivo* (Rosenblatt, Raff and Cramer, 2001; Mysorekar *et al.*, 2002; AbdelRahman and Belland, 2005). Epithelial extrusion is an anti-microbial response that *Chlamydia* must deal with to ensure the completion of its developmental cycle and the formation of infectious particles that enable subsequent rounds of infection. In this report, we described the direct modulation of FAs stability that required the T3SS effector TarP and its interaction with the FA-associated protein vinculin.

Focal adhesion changes were observed throughout infection, as early as 2 hpi, which led to the hypothesis that an EB-associated protein could be involved. TarP was identified as an ideal candidate based on its association with EBs and the presence of binding sites, i.e. LD and VBD for FAK and vinculin, respectively. In this report, it was observed that FA modulation could be observed up to 20 hpi even when chlamydial protein synthesis was inhibited starting at 0 hpi. We propose that TarP is present throughout infection, albeit at developmentally regulated levels to sustain the modulated character of FAs in infected cells. For TarP to sustain its modulation of FAs in infected cells, the protein would have to be either stable from the time it is translocated during invasion and/or synthesized throughout infection. Indeed, using β-lactamase fusions, Mueller and Fields (2015) were able to show constant expression and translocation of TarP from its native promoter throughout infection. We also report that the pool of translocated TarP was relatively stable (Figure S3E). In this experiment, infection of cultured cells was performed in the constant presence of chloramphenicol to prevent *de novo* TarP synthesis. We observed by Western blot that TarP was present up to 24 hpi, the latest time monitored. Thus, it appears that in chloramphenicol-treated infected cells, the enduring presence of TarP correlated with the increase number of FAs phenotype. Furthermore, while relative TarP protein levels during infection decreased mid-stage, it was never absent (Clifton *et al.*, 2004). Importantly, TarP continued to be translocated throughout infection as indicated by reactivity to the anti-phosphotyrosine 4G10 (Mueller and Fields, 2015).

Currently, it is impossible to generate *Chlamydiae* TarP mutants owing to its indispensable role in the invasion process of this obligate intracellular pathogen. It was also technically difficult to locate endogenous translocated TarP molecules likely due to their limiting amount compounded with the significant dilution once in the host cell cytosol, and distribution among the host cell's FAs. Nevertheless, using similar approaches (e.g. ectopic expression) for studies of the subcellular localization of endogenous T3SS effectors, we were able to demonstrate the FA localization of TarP and its crucial role in FA modulation by *Chlamydia*. The FA localization was specific, being dependent on the respective FAK and vinculin binding domains in TarP. A side-by-side comparison of the respective effects of infection and TarP transfection on FAs enabled us to determine the extent of the contribution of TarP to the FA phenotypes. *Chlamydia* infection led to increased numbers and stability of FAs. The latter involved resistance to disassembly induced by treatment with blebbistatin, which is an inhibitor of myosin II (Feng *et al.*, 1999; Wang *et al.*, 2008; Liu *et al.*, 2010). Importantly, TarP makes a significant contribution to the various FA phenotypes observed in infected cells. Based on our TarP transfection studies, $TarP^{1\text{-}1006\Delta625\text{-}650}$, $TarP^{829\text{-}1006}$, $TarP^{829\text{-}929}$, and $TarP^{905\text{-}1006}$ were involved in FA localization. Increased FA numbers were observed in cells ectopically expressing the same four TarP constructs. FAs in cells expressing $TarP^{1\text{-}1006\Delta625\text{-}650}$, $TarP^{829\text{-}1006}$, and $TarP^{905\text{-}1006}$ remained intact during blebbistatin treatment, revealing the role of the VBD motif of TarP. Additionally, only $TarP^{1\text{-}1006\Delta625\text{-}650}$ was able to mimic CtrL2 infection in relation to the recruitment and turnover of FAs. From these experiments, it was determined that TarP's FA targeting domain VBD was sufficient to modulate FA, however other domain(s) in the N-terminus were necessary to fully mimic CtrL2 infection. Resistance of FA to myosin II inhibition required the VBD domain. In short, the VBD motif plays an important role in the modulation of FAs by TarP. We further implicated the TarP-vinculin interaction via the VBD domain in various aspects of FA modulation, specifically FA localization and FA resistance to disassembly by blebbistatin.

How might TarP affect FA stability? TarP does not have any known enzymatic activities, such as phosphorylation. Instead its known roles are as a protein scaffold to which signaling molecules are recruited, and a bacterial actin nucleator (Clifton *et al.*, 2004; Jewett *et al.*, 2006; Lane *et al.*, 2008). The reorganization of FAs observed in TarP-transfected cells is likely to be a

significant determinant of FAs stability. How reorganization translates to stability (i.e. resistance to blebbistatin) is not clear, but that the same domain of TarP being implicated in different FA changes, including the vertical reorganization, indicates an important role for this effector. To our knowledge, changes to the vertical organization of FAs have not been described in any experimental system, and thus, the mechanism for how the reorganization translates to stability is not known. A possibility is the displacement of signaling molecules, disrupting protein-protein interactions essential to normal FA dynamics. The data presented here that demonstrated the essential role of the VBD domain in modifying the vertical organization of FAs is consistent with this idea. It is also possible that the binding of TarP to vinculin may result in the disruption of the interaction between the tail and head domains of vinculin, preventing the inactivation of vinculin in the absence of myosin II mechanical tension. Indeed, in MEFs *vcl*$^{-/-}$ expressing truncated versions of vinculin lacking the tail domain were resistant to the loss of mechanical tension (Carisey *et al.*, 2013). The removal of the tail domain constitutively activated vinculin by preventing its inactivation through self-folding. Additionally, Carisey *et al.*, (2013) also demonstrated that vinculin regulates the release of other FA proteins, such as, talin, paxillin, FAK, ILK, among others. A similar stabilizing mechanism could be involved in CtrL2-dependent FA resistance to the loss of mechanical tension exerted by myosin II. The interaction between TarP and vinculin might prevent its inactivation and consequently stabilizes the FA complexes to the extent that mimics the constitutively activated vinculin.

In this report, we identified a potential virulence strategy of *Chlamydia* that counteracts exfoliation of epithelial cells from the mucosal surface. We quantified the kinetics of focal adhesion formation and turnover, described a novel vertical reorganization phenotype of FAs in infected cells, and identified a type III effector (TarP) and its interacting partner (vinculin) that mediate these changes. TarP was initially identified as an invasion-associated protein, and in this report, we assign to it a post-invasion role, raising new questions, including the extent of the role TarP plays in survival and pathogenesis.

Materials and Methods

Cell culture. Cos7 (ATCC CRL-1651), NIH3T3 (kindly supplied by Hector Aguilar-Carreño ATCC CRL-1658) and HeLa 229 (ATCC CCL-2.1) MEFs *vcl*$^{-/-}$ and matched HeLa 229 MEFs *vcl*$^{+/+}$ (Marg *et al.*, 2010) (were kindly provided by Dr. Wolfgang Ziegler Hannover Medial School).cells were culture using Dulbecco's Modified Eagle Medium (DMEM) (Thermofisher scientific, 11960-085). Media were supplemented with 10% fetal bovine serum (Sigma, F0804-500ML), 2mM L-glutamine, and 10µg/ml gentamicin. The human keratinocytes HaCaT cells (kindly supplied by Dr. Kristin M. Braun) were cultured in 3 parts DMEM and 1 part Ham's F-12 Nutrient Mix (Thermofisher scientific 11765054), supplemented with 10% fetal bovine serum (Sigma, F0804-500ML), 2 mM L-glutamine, 10µg/ml gentamicin, insulin (Sigma I9278-5ML) and hydrocortisone cholera toxin EGF (HCE) cocktail. *Chlamydia trachomatis* serovar L2 (L2/434/Bu) was propagated in HeLa 229. EBs were harvested by discontinuous density gradient centrifugation in gastrografin (Bracco Diagnostics), as previously described (Thwaites *et al.*, 2014).

***Chlamydia* infections.** Cells were infected with *Chlamydia trachomatis* serovar L2 (L2/434/Bu, CtrL2) at the multiplicity of infection MOI of 5, for 20 h, and of 25, for 8 h, in ice cold serum-free DMEM. Cells were centrifuged at 1000 rpm for 5 min at 4 °C to synchronize the infection. After centrifugation, the inoculum was replaced with warm DMEM supplemented with 10% fetal bovine serum, 2 mM L-glutamine, and 10µg/ml gentamicin. In parallel, a mock-infected control was made following the same protocol but without *Chlamydia* infectious particles.

Immunostaining. Cells were grown on Fibronectin coated coverslips (Neuvitro, GG-12-fibronectin) for the duration of the experiment. At the pre-determined, time cells were rinsed with Hank's Balanced Salt Solution (HBSS) (Thermofisher scientific, 14025-100) and fixed using 4% paraformaldehyde (PFA) in PBS pH 7.4 (Gibco, 14190-094) for 20 min at room temperature. The fixed cells were then permeabilized using PBS with 0.2% Triton X-100. Subsequently, permeabilized cells were incubated with 1% BSA (Sigma, A9418) in PBS, for 30 min at room temperature, to block non-specific antigen binding. Cells were then incubated with the primary

antibodies overnight at 4ºC with rocking. The primary antibodies used in this study were rabbit polyclonal antibody against FAK phosphorylated at tyrosine 397 (pFAK-Y397) (Abcam, ab4803), rabbit monoclonal antibody paxillin (Abcam, ab32084), mouse monoclonal antibody vinculin (Abcam, ab18058), Mouse monoclonal Flag-tag antibody (Cell Signalling, 8146S) mouse monoclonal antibody *Chlamydia* LPS (Abcam, ab62708) and convalescent human sera. Afterwards cells were incubated with appropriate fluorescently conjugated secondary antibodies and, when specified, with DAPI (Roche, 10236276001) and Alexa flour 488 phalloidin stains, for 1 hr at room temperature, with rocking. In this study, the following secondary antibodies were used: goat anti-rabbit Alexa flour 488 (Thermofisher Scientific, A11008), goat anti-rabbit Alexa flour 633 (Thermofisher Scientific, A21071), goat anti-mouse Alexa flour 594 (Thermofisher Scientific, A11005), goat anti-human Alexa flour 647 (Thermofisher scientific A-21445). Following staining, the coverslips were mounted with Mowiol, and visualized in ZEISS LSM 710 confocal microscope, in the Microscopy and Histology Core Facility at the University of Aberdeen, or the Leica SP8 confocal microscope in Washington State University Integrative Physiology and Neuroscience advance image equipment. FIJI software (Schindelin *et al.*, 2012; Schneider, Rasband and Eliceiri, 2012) was used to generate the final images.

Time-lapse microscopy. For live-cell imaging of FAs NIH3T3 cells were seeded on ibidi µ-slide 8 well chambers with fibronectin coating (ibidi, 80823) at the recommended seeding density and left overnight in a 37 ºC, 5% CO_2 incubator. The following day, cells were infected with CtrL2 with a MOI of 5. At 2 h post-infection, the cells were transfected with either Vinculin-venus (Grashoff *et al.*, 2010) a gift from Martin Schwartz, (Addgene, 27300), paxillin-pEGFP (Laukaitis *et al.*, 2001) a gift from Rick Horwitz, (Addgene, 15233), or FAK-GFP (Gu *et al.*, 1999; Lane *et al.*, 2008) a gift from Kenneth Yamada, (Addgene, 50515) using Lipofectamine 3000 transfection reagent (Thermofisher Scientific, L3000008), following the manufacture instructions. After 20 to 22 h, time lapsed images of transfected cells were obtained using a Leica SD6000 AF in TIRF mode, in Washington State University IPN advance image equipment. Images of the GFP-tagged proteins were collected every

minute for 90 min. The time lapse images were uploaded to the Focal adhesion Analysis server (Berginski and Gomez, 2013).

***De novo* protein inhibition.** Cos7 cells were cultured as previously described. Prior to infection, cells and EB particles were treated with 60 µg/ml of chloramphenicol (Sigma C0378) for 30 min. Cells and EBs were kept in chloramphenicol supplemented DMEM until fixation. Cells were fixed at 8 or 20 h post-infection and were immunostained as described above.

Cloning and transfection of TarP contructs. A summary of the primers used in this study is provided in Table S1. Initially TarP$^{1\text{-}1006}$, TarP$^{829\text{-}1006}$, TarP$^{829\text{-}929}$ and TarP$^{905\text{-}1006}$ were PCR amplified from CtrL2 genomic DNA using the primers combination 1-2, 5-2, 5-6 and 4-2, respectively. A *Bam*H1 (reverse primer) and *Kpn*I (forward primer) restriction sites were used for fusion with the N1-mturquoise2 plasmid. The TarP$^{1\text{-}1006\Delta650\text{-}625}$ was obtained using the 7-8 primer pair for PCR amplification from TarP$^{1\text{-}1006}$-mturquoise2 fusion plasmid. The primers were created to amplify the whole TarP$^{1\text{-}1006}$-mturquoise2 except the nucleotides that constitute the proline rich domain (PRD) 625-650. The resulting PCR product was recombined using in-Fusion HD cloning plus CE (Clontech, 638916) to create a functional circular plasmid. TarP$^{1\text{-}829\Delta625\text{-}650}$ was PCR amplified from the TarP$^{1\text{-}1006\Delta625\text{-}650}$-mturquoise2 plasmid using the primers pair 1-3. The same restriction enzymes were used to clone these fragments into N1-mturquoise2. Transformations using restriction enzymes recombination were made into chemically competent Top10 (invitrogen) *E. coli*, and vectors sequence was verified using sequencing (Eurofins) The construct pFH-TarP$^{1\text{-}1006\Delta625\text{-}650}$ and pFH-TarP$^{1\text{-}829\Delta625\text{-}650}$ used for super-resolution experiments was PCR amplified from TarP$^{1\text{-}1006\Delta625\text{-}650}$-mturquoise2 using primers combination 9-10 and 9-17, respectively. To use homology cloning the vector backbone 1436 pcDNA3-Flag-HA, kindly provided by William Sellers (Addgene 10792), was linearized by PCR using the primers pair 11-12 and 11-18, creating homology overhang regions to the TarP$^{1\text{-}1006\ \Delta625\text{-}650}$ and TarP$^{1\text{-}829\ \Delta625\text{-}650}$, respectively. TarP$^{829\text{-}1006}$ was amplified from CtrL2 genomic DNA using the primer pairs 13-14. To use homology cloning the vector backbone 1436 pcDNA3-Flag-HA was linearized by PCR using the primer pair 15-16. Fragments and vector

backbone were recombined using in-Fusion HD cloning plus CE (Clontech, 638916) to create a functional circular plasmid. Transformations using homology recombination were made into chemically competent Stellar (Clontech) *E. coli*, and vectors sequence was verified using sequencing (Eurofins). The pcDNA3-Flag-Apex-Nes was a gift from Alice Ting (Addgene, 49386). The N1-mturquoise2 (Addgene, 54843). Transfections were done as described above. For iPALM experiments 1µg of DNA and 2µl of sheared salmon sperm DNA were mixed together in 15µl of Opti-MEM (Thermofisher scientific, 31985062), and kept on ice for 15 min. $1x10^6$ Cos7 cells were resuspended in 200µl of cold Opti-MEM, mixed with the DNA solution and kept on ice for 30 seconds. Cells and DNA suspension were transferred to a 4mm gap cuvette (BioRad, 1652088) and electroporated using BioRad Gene Pulser XCell using the following settings: 190V; 950uF; infinity. After electroporation 1.5ml of warm growth media was added. 400µl of cell solution was added to a 6 well plate well containing 1.5ml of warm growth media and the gold fiducial coverslip. Cells were incubated 37°C, 4% CO_2 for 4 h to adhere to the gold fiducial coverslip. Cells were washed to remove dead cells debris and further incubated for 20 h.

Trypsin assay. Cells were plated in 24 well plates and incubated at 37°C and 5% CO2, until 80-90% confluency. Afterwards, cells were infected with CtrL2 with a multiplicity of infection of 5 for 20 h. Cells were then treated with 0.01% trypsin diluted in serum-free DMEM media at 37°C, for 0, 10, 20, 30, or 35 min. Cells were fixed with 4% PFA, carefully washed with PBS and stained with DAPI to count the number of remaining cells as well as to visualize *Chlamydia* inclusions. Images were taken using Nikon eclipse TE2000-U.

iPALM imaging and analysis. The principle of instrumentation for iPALM imaging and analysis were performed as previously described (Shtengel *et al.*, 2009; Kanchanawong *et al.*, 2010) with the following modifications. After 24°C of transfection cells plated in gold fiducial coverslip were fixed with 0.8% PFA and 0.1% glutaraldehyde (Sigma G7526-10ML) solution (in PBS) for 10 min. After fixation cells were washed 3 times with PBS and quenched using 1% NaBH4 (Sigma, 452882-25G) solution (in PBS) for 7 min. Cells were then washed again 3 times with PBS. After washing

cells were immunostained (when necessary) and/or processed for iPALM imaging as previously described (Kanchanawong *et al.*, 2010). The vertical coordinates relative to the golden fiducial markers are indicating by a color scale from red (0 nm) to purple (250 nm).

Acknowledgments

We would like to thank Dr. Raphael Valdivia (Duke University) for the generous gift of the TarP antibody; Drs. Martin Schwartz, Rick Horwitz, Kenneth Yamada, William Sellers, Alice Ting, and Michael Davidson for various constructs through Addgene; the services provided by the Aberdeen Imaging Facility in the Institute for Medical Sciences and the WSU Integrated Physiology and Neuroscience imaging facilities; and Satya Khuon (AIC Janelia) for technical help and advice. This project was supported by grants from the University of Aberdeen's Knowledge Exchange Transfer Fund, the National Institute for Food and Agriculture (#1010265), National Institutes of Health (AI065545), and start-up funds from the WSU College of Veterinary Medicine to R.A.C. A.T.P. and A.T.N. are recipients of the Fundação para a Ciência e Tecnologia, SFRH/BD/76741/2011 and SFRH/BD/86670/2012, respectively. T.R.T. is a Medical Research Council studentship awardee. iPALM data used in this publication was produced in collaboration with the Advanced Imaging Center, a facility jointly supported by the Gordon and Betty Moore Foundation and Howard Hughes Medical Institute at the Janelia Research Campus.

Author Contributions

Conceptualization, A.T.P., A.T.N. and R.A.C.; Methodology, A.T.P., J.A., and R.A.C.; Software, J.A.; Formal Analysis, A.T.P.; Investigation, A.T.P., A.T.N, J.A., and T.R.T.; Writing – Original Draft, A.T.P., and R.A.C.; Writing – Review & Editing, A.T.P., A.T.N. and R.A.C; Funding Acquisition, A.T.P., A.T.N. and R.A.C.; Resources, J.A., T.L.C. and R.A.C.; Supervision, T.L.C. and R.A.C.

Conflict of Interest

The authors have declared that no competing or financial interests exist.

References

AbdelRahman, Y. M. and Belland, R. J. (2005) 'The chlamydial developmental cycle', *FEMS Microbiology Reviews*, 29(5), pp. 949–959. doi: 10.1016/j.femsre.2005.03.002.

Berginski, M. E. and Gomez, S. M. (2013) 'The Focal Adhesion Analysis Server: a web tool for analyzing focal adhesion dynamics.', *F1000Research*, 2, p. 68. doi: 10.12688/f1000research.2-68.v1.

Betzig, E. *et al.* (2006) 'Imaging Intracellular Fluorescent Proteins at Nanometer Resolution', *Science*, 313(5793), pp. 1642–1645. doi: 10.1126/science.1127344.

Borradori, L. and Sonnenberg, A. (1999) 'Structure and function of hemidesmosomes: More than simple adhesion complexes', *Journal of Investigative Dermatology*. Elsevier Masson SAS, 112(4), pp. 411–418. doi: 10.1046/j.1523-1747.1999.00546.x.

Carisey, A. *et al.* (2013) 'Vinculin regulates the recruitment and release of core focal adhesion proteins in a force-dependent manner.', *Current biology : CB*, 23(4), pp. 271–81. doi: 10.1016/j.cub.2013.01.009.

Clifton, D. R. *et al.* (2004) 'A chlamydial type III translocated protein is tyrosine-phosphorylated at the site of entry and associated with recruitment of actin.', *Proceedings of the National Academy of Sciences of the United States of America*, 101(27), pp. 10166–71. doi: 10.1073/pnas.0402829101.

Feng, J. *et al.* (1999) 'Inhibitory Phosphorylation Site for Rho-associated Kinase on Smooth Muscle Myosin Phosphatase', *Journal of Biological Chemistry*, 274(52), pp. 37385–37390. doi: 10.1074/jbc.274.52.37385.

Geiger, B. *et al.* (2001) 'Transmembrane crosstalk between the extracellular matrix--cytoskeleton crosstalk.', *Nature reviews. Molecular cell biology*, 2(11), pp. 793–805. doi: 10.1038/35099066.

Grashoff, C. *et al.* (2010) 'Measuring mechanical tension across vinculin reveals regulation of focal adhesion dynamics.', *Nature*, 466(7303), pp. 263–6. doi: 10.1038/nature09198.

Gu, J. *et al.* (1999) 'Shc and FAK differentially regulate cell motility and directionality modulated by PTEN.', *The Journal of cell biology*, 146(2), pp. 389–403. Available at: http://www.pubmedcentral.nih.gov/articlerender.fcgi?artid=2156182&tool=pmcentrez&rendertype=abstract (Accessed: 23 February 2016).

615 Heymann, J. *et al.* (2013) 'Chlamydia trachomatis infection prevents front-rear polarity of migrating
616 HeLa cells', *Cellular Microbiology*, 15(7), pp. 1059–1069. doi: 10.1111/cmi.12114.
617 Jewett, T. J. *et al.* (2006) 'Chlamydial TARP is a bacterial nucleator of actin.', *Proceedings of the*
618 *National Academy of Sciences of the United States of America*, 103(42)(42), pp. 15599–15604. doi:
619 10.1073/pnas.0603044103.
620 Kanchanawong, P. *et al.* (2010) 'Nanoscale architecture of integrin-based cell adhesions.', *Nature*.
621 Nature Publishing Group, 468(7323), pp. 580–584. doi: 10.1038/nature09621.
622 Kim, D.-H. and Wirtz, D. (2013) 'Focal adhesion size uniquely predicts cell migration', *The FASEB*
623 *Journal*, 27(4), pp. 1351–1361. doi: 10.1096/fj.12-220160.
624 Kim, M. *et al.* (2009) 'Bacteria hijack integrin-linked kinase to stabilize focal adhesions and block
625 cell detachment.', *Nature*, 459(7246), pp. 578–582. doi: 10.1038/nature07952.
626 Kim, M. *et al.* (2010) 'Reinforcement of epithelial cell adhesion to basement membrane by a
627 bacterial pathogen as a new infectious stratagem', *Virulence*, 1(April 2010), pp. 52–55. doi:
628 10.1038/nature07952.he.
629 Kumar, Y. and Valdivia, R. H. (2008) 'Reorganization of the host cytoskeleton by the intracellular
630 pathogen Chlamydia trachomatis', *Commun Integr Biol*, 1(2), pp. 175–177. doi:
631 10.1016/j.chom.2008.05.018.www.landesbioscience.com.
632 Lane, B. J. *et al.* (2008) 'Chlamydial entry involves TARP binding of guanine nucleotide exchange
633 factors', *PLoS Pathogens*, 4(3). doi: 10.1371/journal.ppat.1000014.
634 Laukaitis, C. M. *et al.* (2001) 'Differential dynamics of alpha 5 integrin, paxillin, and alpha-actinin
635 during formation and disassembly of adhesions in migrating cells.', *The Journal of cell biology*,
636 153(7), pp. 1427–40. Available at:
637 http://www.pubmedcentral.nih.gov/articlerender.fcgi?artid=2150721&tool=pmcentrez&rendertype=a
638 bstract (Accessed: 23 February 2016).
639 Liu, Z. *et al.* (2010) 'Blebbistatin inhibits contraction and accelerates migration in mouse hepatic
640 stellate cells.', *British journal of pharmacology*, 159(2), pp. 304–15. doi: 10.1111/j.1476-
641 5381.2009.00477.x.
642 Marg, S. *et al.* (2010) 'The Vinculin-ΔIn20/21 Mouse Characteristics of a Constitutive, Actin-Binding

643 Deficient Splice Variant of Vinculin', *PloS one*, 5(7), p. e11530. doi: 10.1371/journal.pone.0011530.
644 Morita-Ishihara, T. *et al.* (2013) 'EspO1-2 Regulates EspM2-Mediated RhoA Activity to Stabilize
645 Formation of Focal Adhesions in Enterohemorrhagic Escherichia coli-Infected Host Cells', *PLoS*
646 *ONE*, 8(2). doi: 10.1371/journal.pone.0055960.
647 Mueller, K. E. and Fields, K. A. (2015) 'Application of b-lactamase reporter fusions as an indicator of
648 effector protein secretion during infections with the obligate intracellular pathogen Chlamydia
649 trachomatis', *PLoS ONE*, 10(8), pp. 1–18. doi: 10.1371/journal.pone.0135295.
650 Mysorekar, I. U. *et al.* (2002) 'Molecular regulation of urothelial renewal and host defenses during
651 infection with uropathogenic Escherichia coli.', *The Journal of biological chemistry*, 277(9), pp.
652 7412–9. doi: 10.1074/jbc.M110560200.
653 Nagano, M. *et al.* (2012) 'Turnover of focal adhesions and cancer cell migration', *International*
654 *Journal of Cell Biology*, 2012. doi: 10.1155/2012/310616.
655 Rosenblatt, J., Raff, M. C. and Cramer, L. P. (2001) 'An epithelial cell destined for apoptosis signals
656 its neighbors to extrude it by an actin- and myosin-dependent mechanism', *Current Biology*, 11(23),
657 pp. 1847–1857. doi: 10.1016/S0960-9822(01)00587-5.
658 Schindelin, J. *et al.* (2012) 'Fiji: an open-source platform for biological-image analysis.', *Nature*
659 *methods*, 9(7), pp. 676–82. doi: 10.1038/nmeth.2019.
660 Schneider, C. A., Rasband, W. S. and Eliceiri, K. W. (2012) 'NIH Image to ImageJ: 25 years of
661 image analysis.', *Nature methods*, 9(7), pp. 671–5. Available at:
662 http://www.ncbi.nlm.nih.gov/pubmed/22930834 (Accessed: 17 July 2014).
663 Shames, S. R. R. *et al.* (2010) 'The pathogenic E. coli type III effector EspZ interacts with host
664 CD98 and facilitates host cell prosurvival signalling', *Cellular Microbiology*, 12(9), pp. 1322–1339.
665 doi: 10.1111/j.1462-5822.2010.01470.x.
666 Shtengel, G. *et al.* (2009) 'Interferometric fluorescent super-resolution microscopy resolves 3D
667 cellular ultrastructure.', *Proceedings of the National Academy of Sciences of the United States of*
668 *America*, 106(9), pp. 3125–3130. doi: 10.1073/pnas.0813131106.
669 Straight, A. F. *et al.* (2003) 'Dissecting temporal and spatial control of cytokinesis with a myosin II
670 Inhibitor.', *Science (New York, N.Y.)*, 299(5613), pp. 1743–7. doi: 10.1126/science.1081412.

671 Thwaites, T. *et al.* (2014) 'The Chlamydia effector TarP mimics the mammalian leucine-aspartic
672 acid motif of paxillin to subvert the focal adhesion kinase during invasion', *Journal of Biological*
673 *Chemistry*, 289(44), pp. 30426–30442. doi: 10.1074/jbc.M114.604876.
674 Thwaites, T. R. *et al.* (2015) 'Vinculin Interacts with the Chlamydia Effector TarP Via a Tripartite
675 Vinculin Binding Domain to Mediate Actin Recruitment and Assembly at the Plasma Membrane',
676 *Frontiers in Cellular and Infection Microbiology*, 5(November). doi: 10.3389/fcimb.2015.00088.
677 Vossenkämper, A., Macdonald, T. T. T. and Marchès, O. (2011) 'Always one step ahead: How
678 pathogenic bacteria use the type III secretion system to manipulate the intestinal mucosal immune
679 system.', *Journal of inflammation (London, England)*. BioMed Central Ltd, 8(1), p. 11. doi:
680 10.1186/1476-9255-8-11.
681 Wang, H. H. H. *et al.* (2008) 'Blebbistatin inhibits the chemotaxis of vascular smooth muscle cells by
682 disrupting the myosin II-actin interaction.', *American journal of physiology. Heart and circulatory*
683 *physiology*, 294(5), pp. H2060–H2068. doi: 10.1152/ajpheart.00970.2007.
684 Zaidel-Bar, R. *et al.* (2007) 'Functional atlas of the integrin adhesome.', *Nature cell biology*, 9(8), pp.
685 858–67. doi: 10.1038/ncb0807-858.
686

687 ## Figure legends

688

689 **Figure 1.** *Chlamydia* infection of confluent monolayers confers resistance to detachment by
690 trypsinization. HeLa cells were infected with CtrL2 or mock-infected for 20 h prior to the start of the
691 experiment. Cells were treated with 0.01% trypsin for the different time points. (A) Cells were
692 visualised by immunostaining of the nuclei and the chlamydial inclusions using DAPI (white).
693 Infected cells are indicated by red arrows. Scale bar: 100 µm. Representative figure of 2
694 independent experiments. (B) The number of nuclei per field of view was counted and data is
695 represented as box-and-whisker plots. Whiskers represent the lowest and highest data point still
696 within 1.5 times the interquartile range. The light blue asterisks indicate significant difference
697 relative to the 0 min time point of each condition (Wilcoxon rank sum test ** = $p<0.01$, *** =
698 $p<0.001$). The dark blue asterisks indicate significant differences between the mock-infected control
699 and C. trachomatis L2 infected at the same time point. The black cross shows the average for each
700 experimental samplel.

701

702 **Figure 2.** *C. trachomatis* increases host cell focal adhesion numbers independently of chlamydial
703 *de novo* protein synthesis. CtrL2 infection increases the numbers of focal adhesions marked by
704 vinculin (A, C) and paxillin (B, D). Cos7 cells infected or mock-infected were monitored at 8 or 20
705 hpi with and without Chloramphenicol for changes to focal adhesions marked by vinculin (A) and
706 paxillin (B), all in green. *Chlamydia* is shown in red. Infected cells showed increased numbers of FA
707 markers when compared to mock-infected cells (top row) in both time points and in chloramphenicol
708 treatment. Scale bar length 10µm. The number of vinculin (C) and paxillin (D) stained focal
709 adhesions in infected and mock-infected cells were counted and data is represented as box-and-
710 whisker plots. Whiskers represent the lowest and highest data point still within 1.5 times the
711 interquartile range. The light blue asterisks indicate significant difference relative to the mock-
712 infected control (Wilcoxon rank sum test ** = $p<0.01$, *** = $p<0.001$). The black cross shows the
713 average for each experimental sample.

714

715 **Figure 3.** Quantitative analyses reveal significant changes to the dynamics of focal adhesion in
716 infected cells. (A-C) NIH3T3 cells CtrL2-infected or mock-infected were transfected with different
717 GFP-tagged constructs of FAK, paxillin or vinculin, and monitored between 20 to 22 hpi for 90 min.
718 (A) Visualization of example cells for paxillin-pEGFP focal adhesion marker. See Figure S2E for
719 example of cells transfected with FAK-pEGFP and vinculin-venus focal adhesion markers. All focal
720 adhesions detected in each frame were given a color ranging from blue (first frame) to red (last
721 frame). Scale bar length 10 µm. (B) and (C) are box-and-whiskers plots that quantify the effect of
722 *Chlamydia* infection on focal adhesion, specifically the recruitment (B) and turnover (C) of focal
723 adhesions labeled with FAK, paxillin, or vinculin. Whiskers represent the lowest and highest data
724 point still within 1.5 times the interquartile range. For statistical analyses the Wilcoxon Rank sum
725 test was used (*** = $p<0.001$). See Figure S2F for DIC images showing the presence or absence of
726 CtrL2 inclusions of example cells. (D, E) *Chlamydia* infected cells are resistant to blebbistatin. Cos7
727 cells were mock-infected (top panels) or infected with CtrL2 for 8 (bottom panels) and 20 h (see
728 Figure S3A and S3B). Cells were fixed and stained for the focal adhesion marker paxillin (in green),
729 F-actin (in red) and human serum for *C. trachomatis* (white). Cells were also mock- (D) or pre-
730 treated (E) with chloramphenicol (Cm) followed by infection of live EBs. The Cm treatment was
731 maintained for the duration of the experiment. Cells without blebbistatin treatment showed clear F-
732 actin stress fibres and paxillin-labeled focal adhesions. (D) Cells were mock treated (first and third
733 row) or treated with 10µM of blebbistatin for 1 h (second and fourth row) to inhibit myosin II
734 contractibility. Scale bar length is 10µm.
735
736 **Figure 4.** The VBD domain ($TarP^{905-1006}$) of TarP is required for its specific focal adhesion
737 localization. (A) Representation of *C. trachomatis* effector protein TarP and its known domains
738 fused to mturquoise2 fluorescent protein. (B) Cos7 cells were transfected with different
739 mturquoise2-tagged TarP constructs (green) and evaluated for effects on focal adhesion numbers
740 (paxillin in red). Phalloidin was used to stain F-actin (blue). Cells were transfected for 20 h at the
741 time of fixation. Scale bar length 10µm. (C) Focal adhesion numbers of cells transfected with the
742 different TarP constructs were quantified and are represented as a box-and-whiskers plot. Whiskers

represent the lowest and highest data point still within 1.5 times the interquartile range. The light blue asterisks indicate significance relative to the N1-mturquoise2 empty vector control (Wilcoxon runk sum test ***=p<0.001). Constructs which were statistically different from the empty-vector control were also compared with TarP$^{1\text{-}1006\Delta625\text{-}650}$, indicated by the dark blue asterisks (Wilcoxon runk sum test *** = p<0.001). The black cross shows the average for each experimental sample.

Figure 5. The VBD domain (TarP$^{905\text{-}1006}$) of TarP is required for focal adhesion resistance to blebbistatin treatment. (A) Cos7 cells were transfected with different mturquoise2-tagged TarP constructs (green) and evaluated for effects on focal adhesion numbers (paxillin in red). Phalloidin was used to stain F-actin (blue). Cos7 cells were transfected for 19 h and then treated with 10 μM of blebbistatin for 1 hr. Scale bar length 10μm. (B, C) NIH3T3 cells were cotransfected with different different mturquoise2-tagged TarP constructs and mcherry-tagged paxillin, and monitored between 20 to 22 h post-transfection for 90 min. See Figure S3D and Movies S5-S10 for example images of NIH3T3 cotransfected cells. Box-and-whiskers plot was used to represent recruitment (B) and turnover (C) of paxillin-mcherry FAs in cotransfected cells. Whiskers represent the lowest and highest data point still within 1.5 times the interquartile range. The light blue asterisks indicate significance relative to the N1-mturquoise2 empty vector control (Wilcoxon runk sum test ***=p<0.001). The black cross shows the average for each experimental sample.

Figure 6. Vinculin is required for *C. trachomatis* L2 and TarP-induced resistance to blebbistatin. MEFs *vcl*$^{+/+}$ (A) and *vcl*$^{-/-}$ (B) cells were mock-infected (top panels) or infected with CtrL2 for 8 h (bottom panels). White asterisk mark CtrL2-infected cells. Cells were fixed and stained for the focal adhesion marker paxillin (in green), F-actin (in red) and human serum for *C. trachomatis* (white). MEFs *vcl*$^{+/+}$ (C) and *vcl*$^{-/-}$ (D) cells were transfected with N1-mturquoise2 or TarP$^{905\text{-}1006}$ (VBD domain) (see Figure S4 for remaining TarP constructs). Cells were fixed and stained for the focal adhesion marker paxillin (in red) and F-actin (in blue). (A-D) Cells were mock-treated (first and third row) or treated with 10μM of blebbistatin for 1 h (second and fourth row) to inhibit myosin II

770 contractibility. Cells without blebbistatin treatment showed clear F-actin stress fibres and paxillin-
771 labeled focal adhesions. Scale bar length is 10μm.
772
773 **Figure 7.** Chlamydia alters the nanoscale architecture of focal adhesions. Cos7 cells transfected
774 with paxillin-tdEos (A, B), FAK-tdEos (C, D) and vinculin (E, F) using electroporation, and seeded
775 on gold fiducial coverslip. (A-F) Top panel shows the top view of area around the example focal
776 adhesion (white boxes). Middle panels display a top view of the example focal adhesion. Bottom
777 panel shows the side view and corresponding z histograms. CtrL2-infected samples display altered
778 vertical (z) organization for paxillin and FAK proteins. The artificial colors are z coordinates for a
779 particular protein in comparison with the fiducial markers (z=0nm, red). Red scale bar length 1μm.
780 see Figure S5 for DIC image of the corresponding cells. White scale bar length 200nm.
781
782 **Figure 8.** TarP-targeted focal adhesions display altered nanoscale architecture. Cos7 cells were
783 cotransfected with $TarP^{1\text{-}1006\Delta625\text{-}650}$ and paxillin-tdEos (A, B), $TarP^{905\text{-}1006}$ and paxillin-tdEos (D, E),
784 or with TarP1-829Δ^{PRD} and paxillin-tdEos (F) using electroporation, and seed on gold fiducial
785 coverslip. (A-F) Top panel shows the top view of area around the example focal adhesion (white
786 boxes). Middle panels display a top view of the example focal adhesion. Bottom panel shows the
787 side view and corresponding z histograms. Cells transfected with *Chlamydia* effector TarP variants
788 that possess the LDVBD domains ($TarP^{1\text{-}1006\Delta625\text{-}650}$ and $TarP^{905\text{-}1006}$) display altered vertical (z)
789 organization. The artificial colors are z coordinates for a particular protein in comparison with the
790 fiducial markers (z=0nm, red). Red scale bar length 1μm. see Figure S5 for DIC image of the
791 corresponding cells. White scale bar length 200nm.
792

A

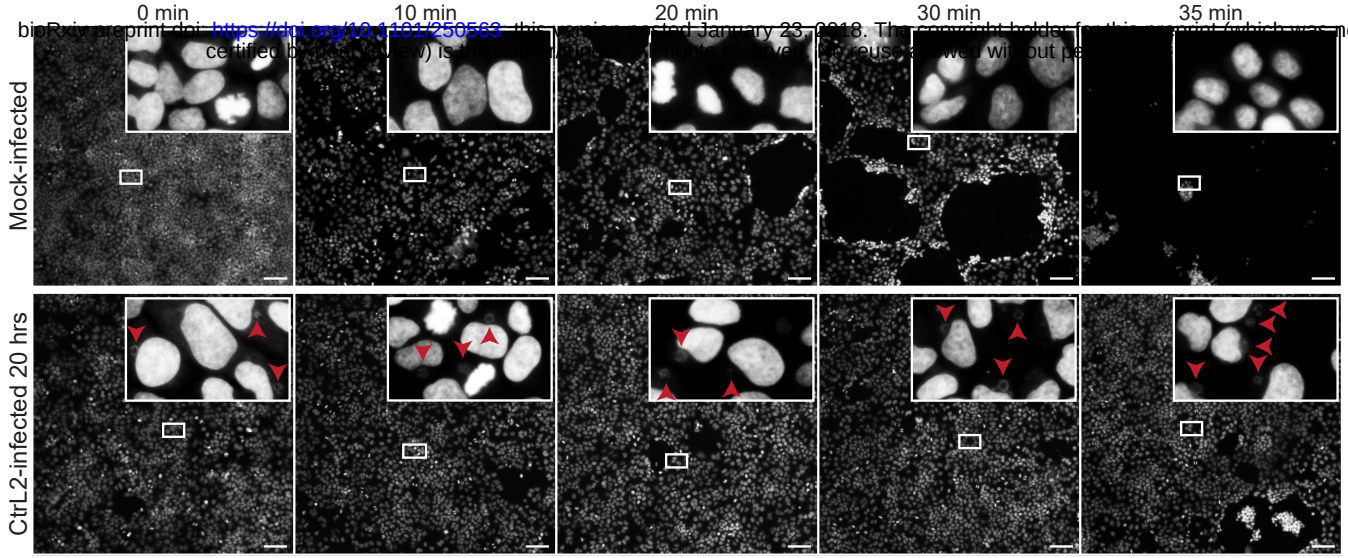

B

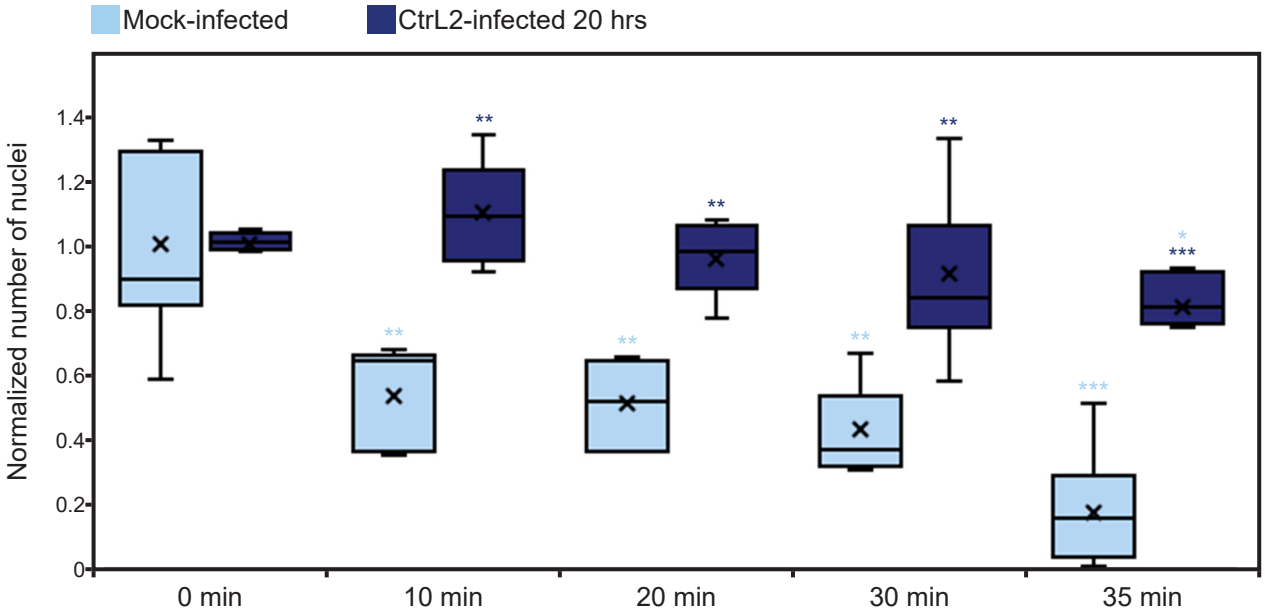

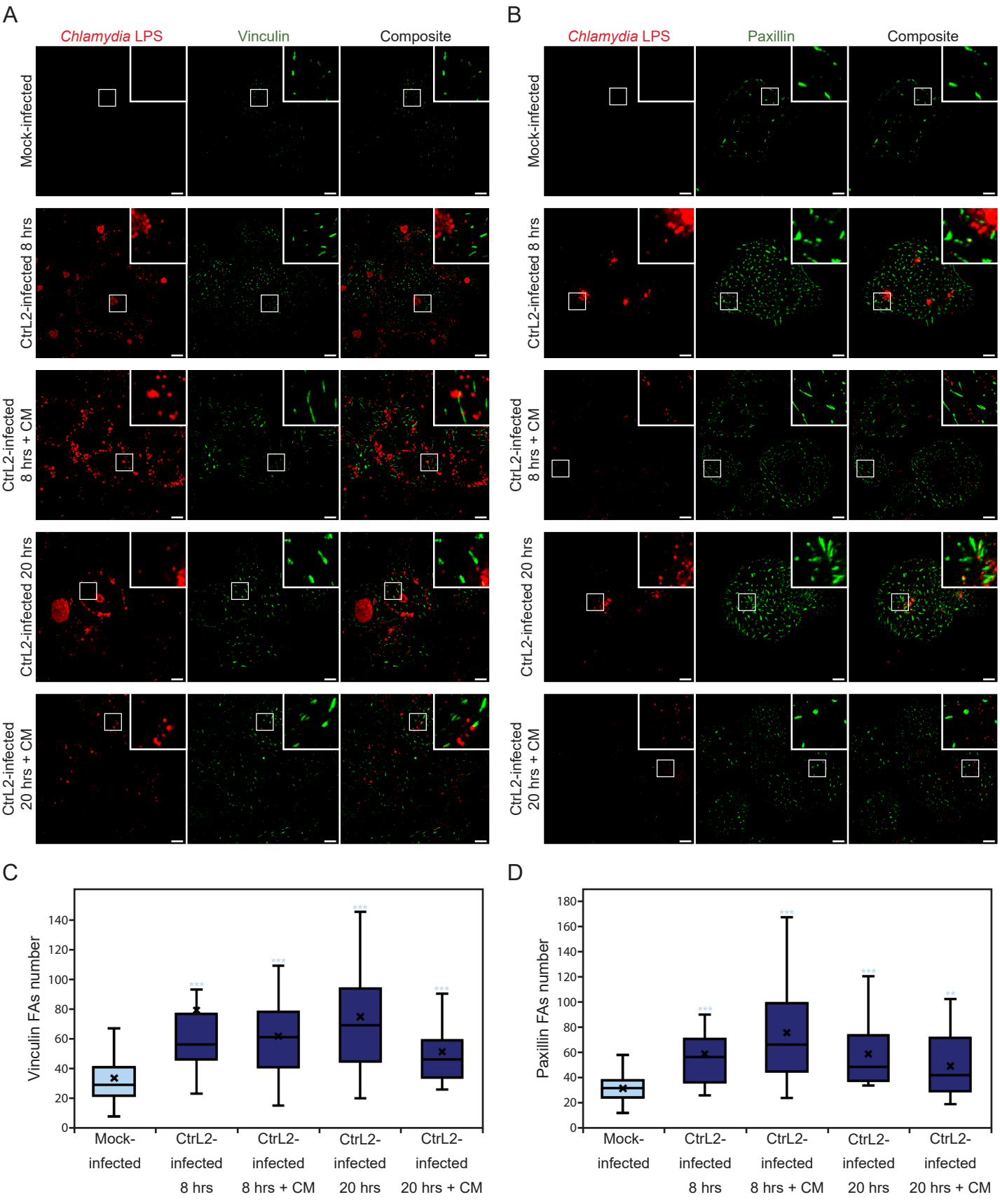

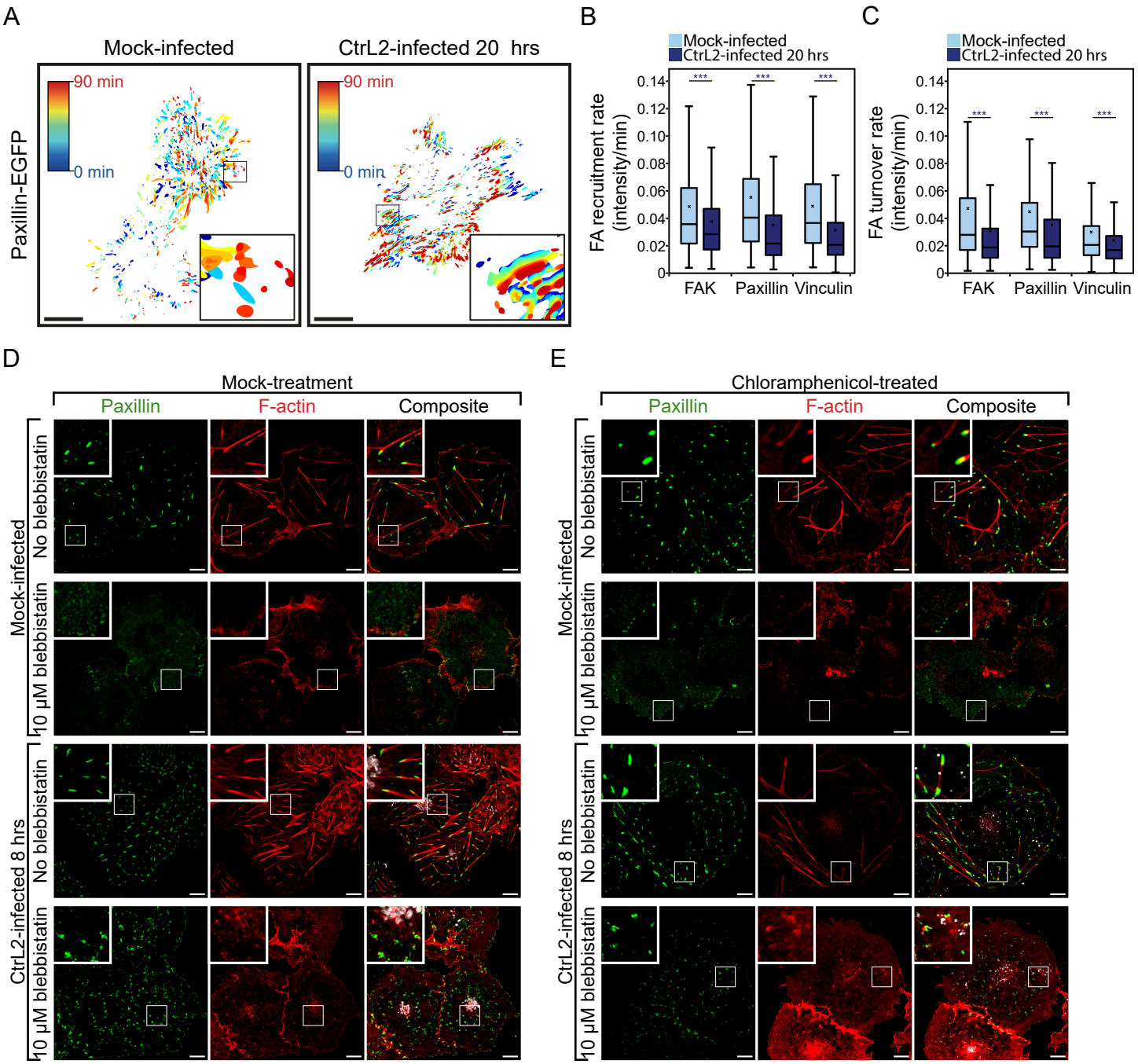

A

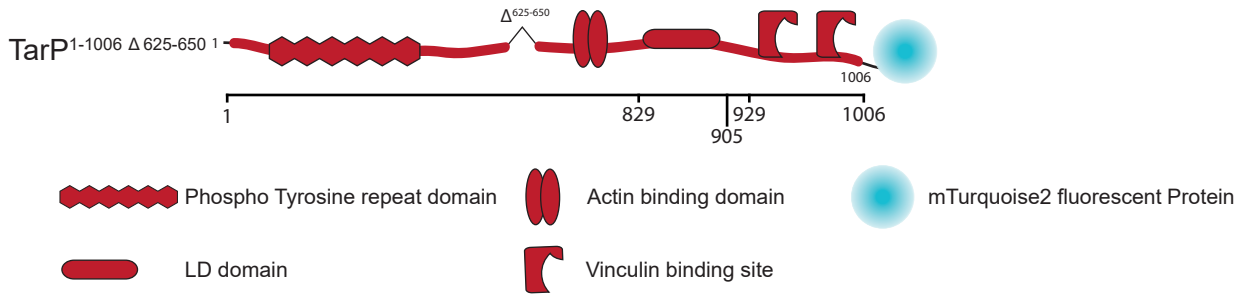

B

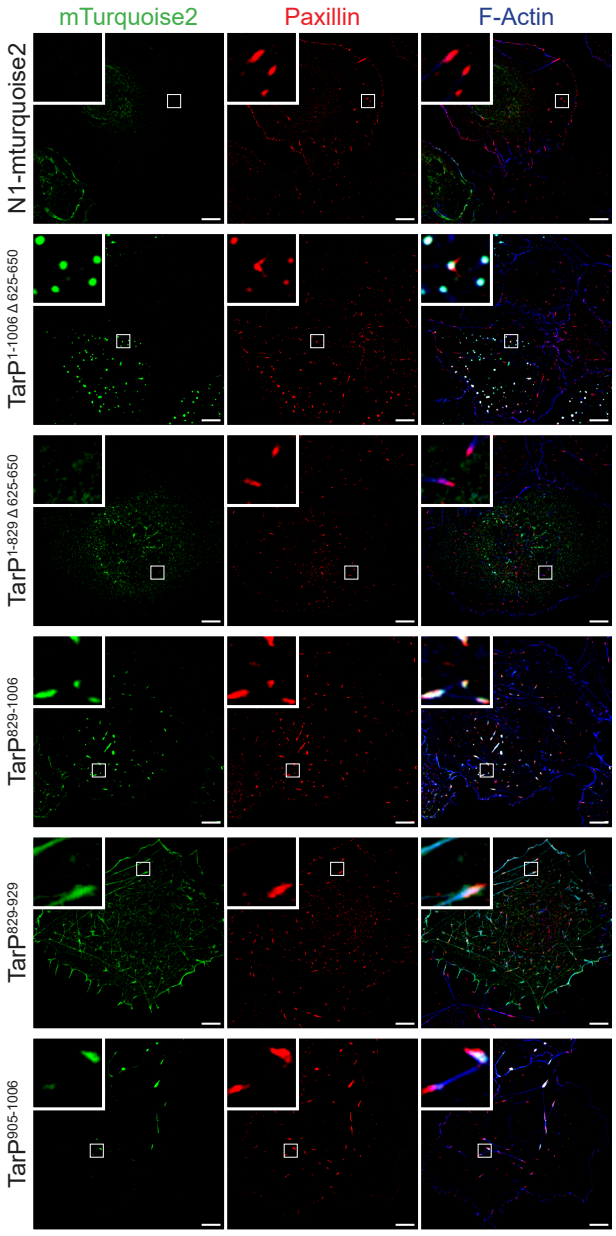

C

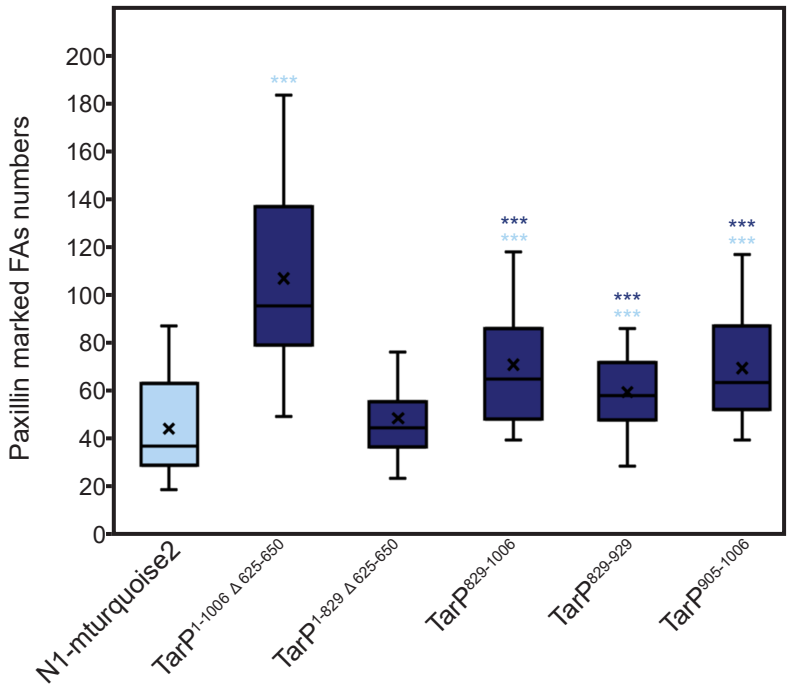

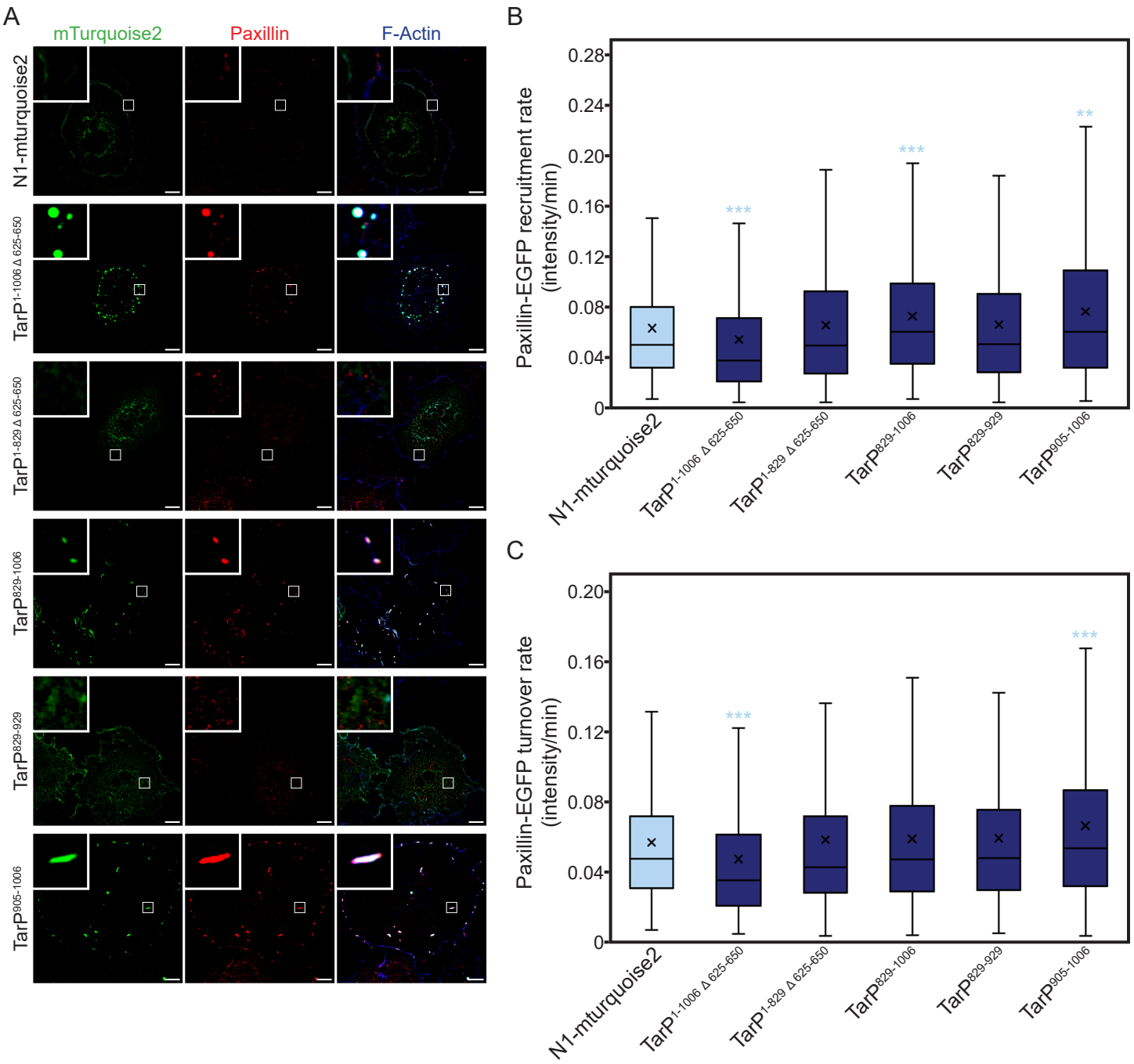

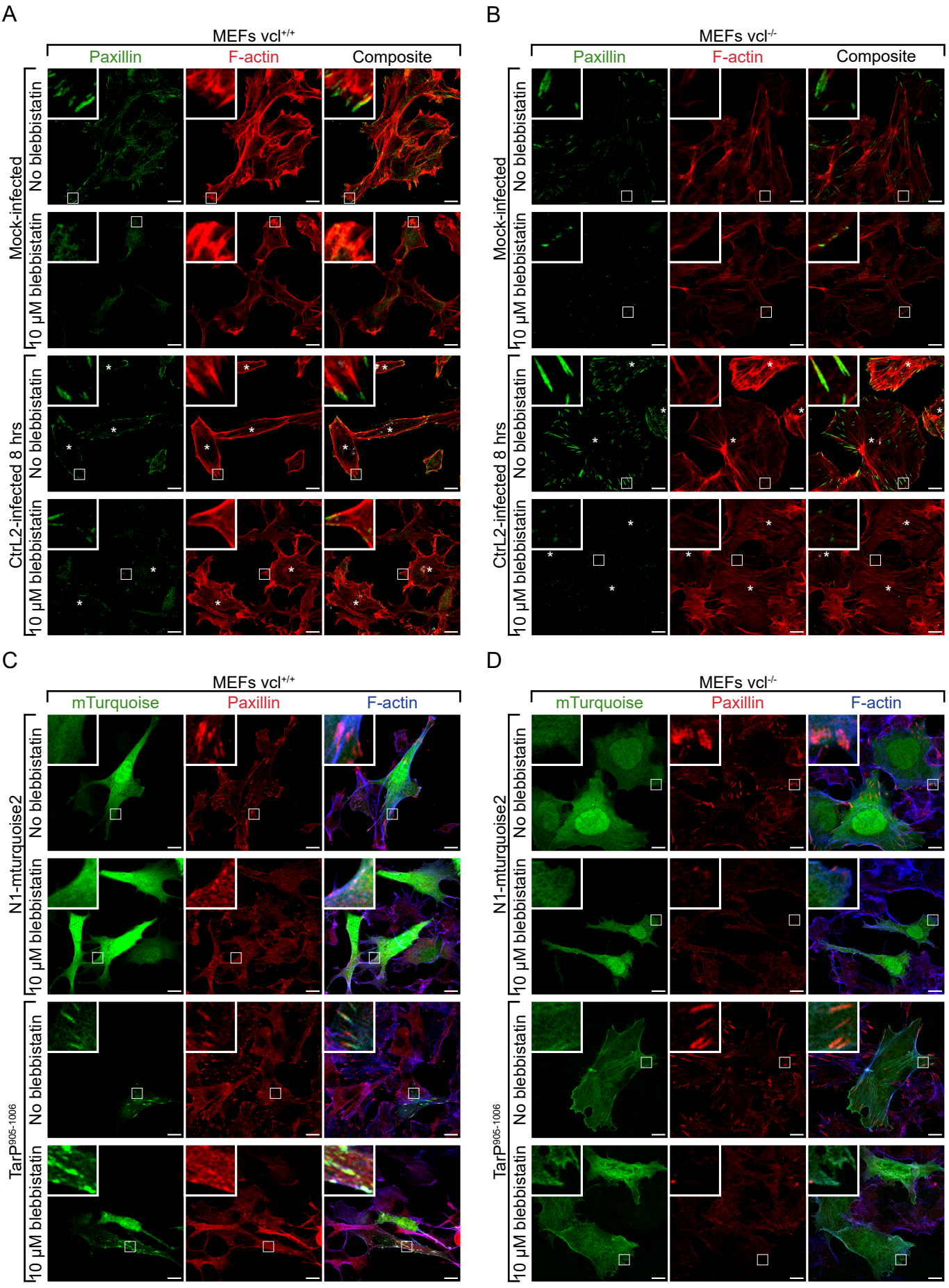

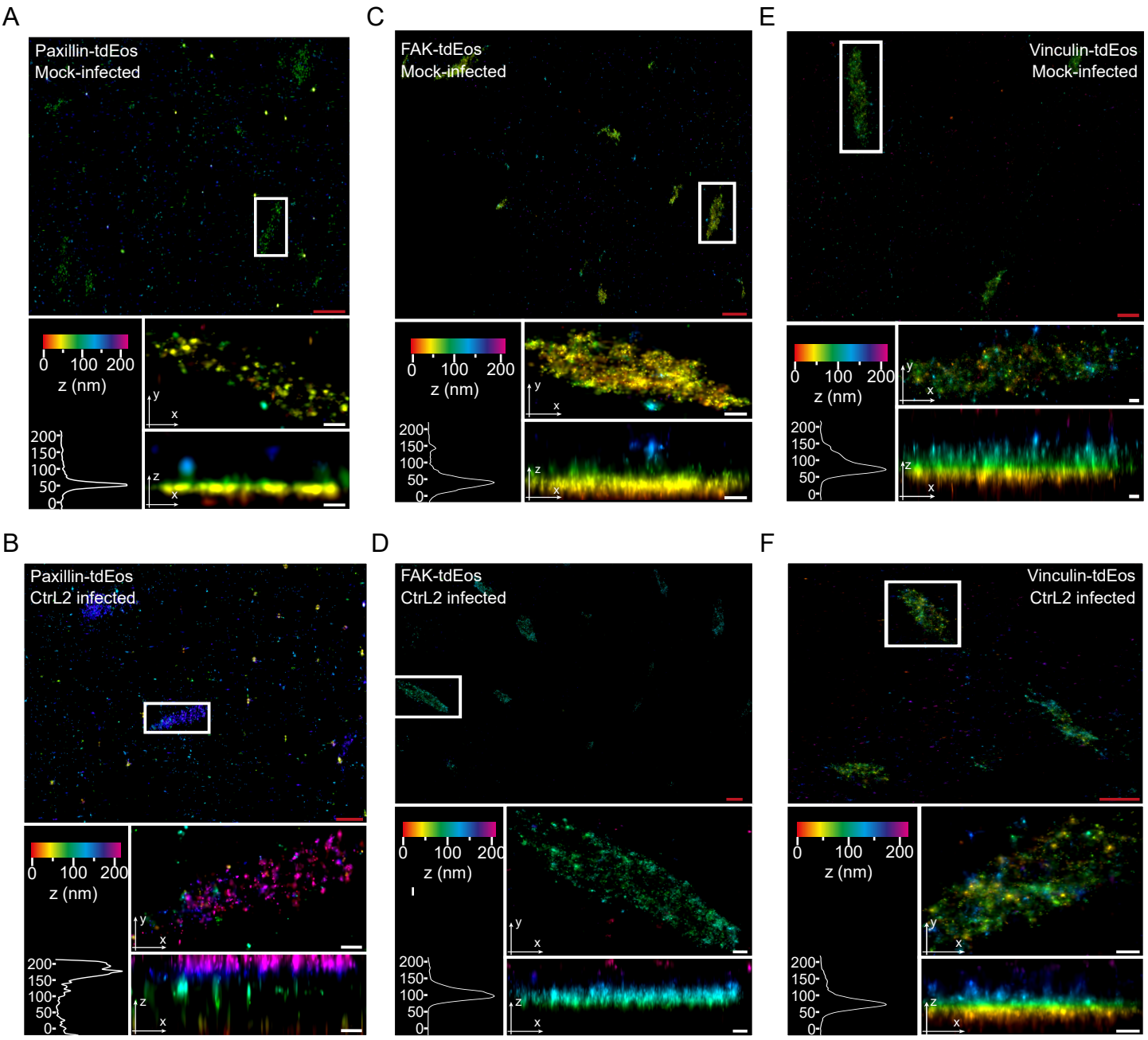

A

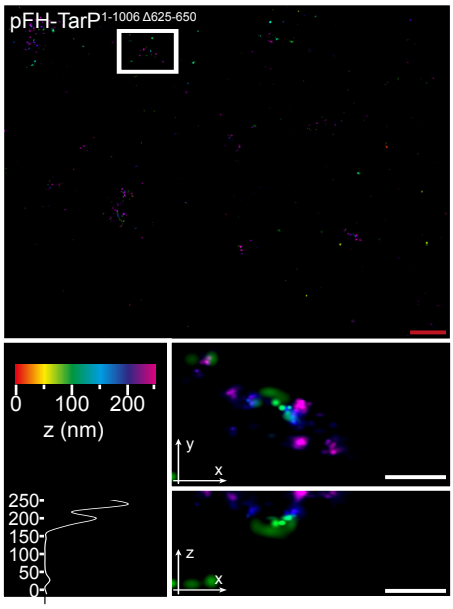

C

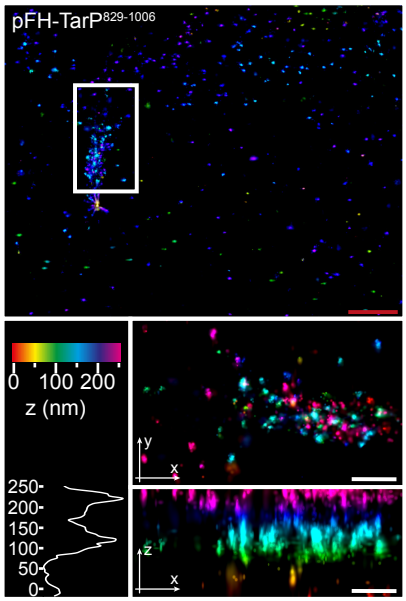

E

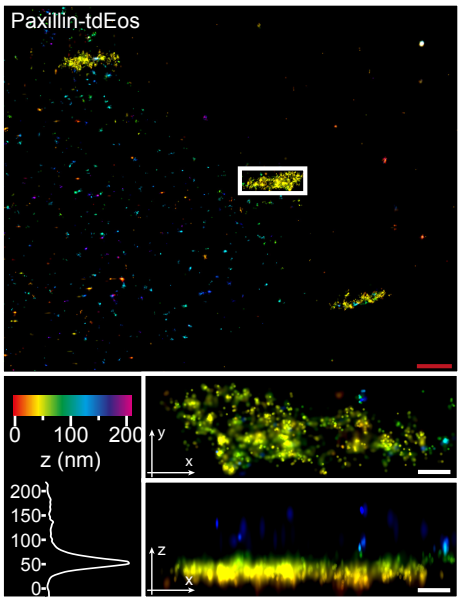

B

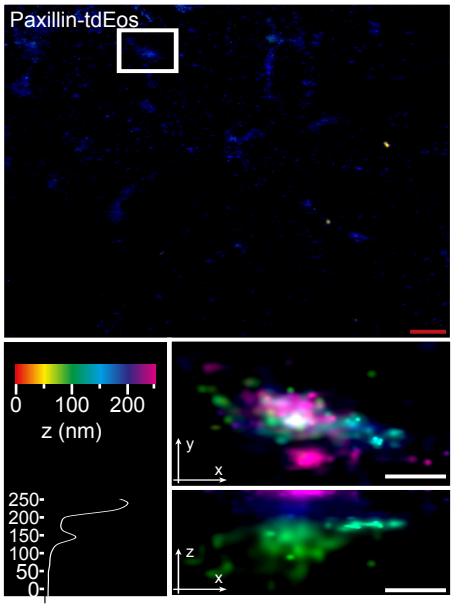

D